

# AFM-based High-Throughput Nanomechanical Screening of Single Extracellular Vesicles

Andrea Ridolfi<sup>1,2,3</sup>, Marco Brucale<sup>\*1,2</sup>, Costanza Montis<sup>1,3</sup>, Lucrezia Caselli<sup>3</sup>, Lucia Paolini<sup>1,4</sup>, Anne Borup<sup>5</sup>, Anders T. Boysen<sup>5</sup>, Francesca Loria<sup>6</sup>, Martijn J. C. van Herwijnen<sup>7</sup>, Marije Kleinjan<sup>7</sup>, Peter Nejsum<sup>5</sup>, Natasa Zarovni<sup>6</sup>, Marca H. M. Wauben<sup>7</sup>, Debora Berti<sup>1,3</sup>, Paolo Bergese<sup>1,4</sup>, Francesco Valle<sup>\*1,2</sup>

<sup>1</sup> Consorzio Interuniversitario per lo Sviluppo dei Sistemi a Grande Interfase (CSGI), Firenze, Italy

<sup>2</sup> Consiglio Nazionale delle Ricerche, Istituto per lo Studio dei Materiali Nanostrutturati (CNR-ISMN), Bologna, Italy

<sup>3</sup> Dipartimento di Chimica "Ugo Schiff", Università degli Studi di Firenze, Firenze, Italy

<sup>4</sup> Dipartimento di Medicina Molecolare e Traslazionale, Università degli Studi di Brescia, Brescia, Italy

<sup>5</sup> Department of Clinical Medicine, Faculty of Health, Aarhus University, Aarhus, Denmark

<sup>6</sup> HansaBiomed Life Sciences, Tallinn, Estonia

<sup>7</sup> Department of Biochemistry & Cell Biology, Faculty of Veterinary Medicine, Utrecht University, Utrecht, The Netherlands

## *Table of contents:*

Experimental details, materials and methods on vesicle preparation, purification and immobilization	Page S2
Experimental details, materials and methods on AFM setup, imaging and force spectroscopy measurements	Page S4
Trigonometry calculations	Page S6
Mechanical characterization of individual vesicles by AFM force spectroscopy (Figure S1)	Page S7
AFM imaging and morphometry analysis (Figure S2)	Page S9
Influence of AFM probe on the nanomechanical characterization of vesicles (Figure S3)	Page S11
Robustness of the image analysis procedure with respect to imaging quality (Figure S4)	Page S13
Dynamic Light Scattering (DLS) and Zeta Potential characterization of synthetic liposomes (Figure S5)	Page S15
Additional EV characterizations	Page S16
EV total molar concentration (Supplementary Table S1)	Page S17
Nanoparticle tracking analysis of EVs (Figures S6, S7, S8)	Page S17
Biochemical characterization of EVs	Page S18
Western blot characterization of purified milk EVs (Figure S9)	Page S19
Supplementary references	Page S20

## *Experimental details, materials and methods*

### ***Liposomes Preparation and Characterization***

Different lipids with PC polar headgroup (DOPC (1,2-dioleoyl-sn-glycero-3-phosphocholine), POPC (1-palmitoyl-2-oleoyl-glycero-3-phosphocholine), DPPC (1,2-dipalmitoyl-sn-glycero-3-phosphocholine), DSPC (1,2-1,2-distearoyl-sn-glycero-3-phosphocholine)) were purchased from Sigma Aldrich (St. Louis, MO, USA); lipid dry powders were dispersed in defined amounts of chloroform, to prepare stock solutions. Lipid films were obtained by evaporating appropriate amounts of lipid stock solutions in chloroform under a stream of nitrogen, followed by overnight drying under vacuum. The films were swollen by suspension in warm (50 °C) milliQ water to a final lipid concentration of 4 mg/mL, followed by vigorous vortex mixing. The dispersions were then tip-sonicated for 15min to obtain a dispersion of unilamellar lipid vesicles. The size distribution and Zeta Potential of the vesicles was determined through Dynamic Light Scattering and Zeta Potential measurements, respectively (see Figure S5).

### ***Natural Vesicles Isolation and Purification***

EVs from Human Colorectal Carcinoma cell line HCT116 were obtained from HansaBioMed Life Sciences Ltd. (Cat. HBM-HCT-30/2); EVs from other natural sources were enriched as described below. All EV data were acquired and reported following MISEV 2018 and MIRABEL international guidelines [Faria 2018; They 2018]. Relevant data were also submitted to the EV-TRACK [Van Deun 2017] knowledge base (EV-TRACK ID: EV190077).

### ***EVs from bovine milk***

Raw milk (100 ml) was collected from the cooled tank from a local dairy farm (Tolakker, Utrecht, The Netherlands), transferred to 50 ml polypropylene tubes and centrifuged for 10 minutes at 22°C at 3000 xg (Beckman Coulter Allegra X-12R, Fullerton, CA, USA). After removal of the cream layer, the milk supernatant was harvested without disturbing the pellet and transferred to new tubes. A second centrifugation step at 3000 xg followed, after which the milk supernatant was collected and stored at -80°C until further processing. Thawed milk supernatant (80 ml) was transferred to polyallomer SW40 tubes (Beckman Coulter) and centrifuged at 5000 xg for 30 minutes at 4°C and subsequently at 10000 xg (Beckman Coulter Optima L-90K with a SW40Ti rotor). For the precipitation of caseins, the milk supernatant was acidified to pH 4.6 by adding Hydrochloric acid (HCl, 1M) while stirring. Caseins were pelleted by centrifugation at 360 xg (Beckman Coulter Allegra X-12R) after which casein-free milk supernatant was collected. Next, 6.5 ml of the milk 10000 xg supernatant was loaded on top of a 60% – 10% Optiprep gradient (Optiprep™, Progen Biotechnik GmbH, Heidelberg, Germany) made in a SW40 tube. Gradients were ultracentrifuged at 197000 xg (Beckman Coulter Optima L-90K with a SW40Ti rotor) for 15-18 h. After centrifugation, fractions of 500 µl were harvested and densities were measured in order to identify the EV-containing fractions with 1.06-1.19 g/ml, which were pooled. Optiprep was exchanged for PBS by using size exclusion chromatography on the EV-containing fractions pooled in a 20 ml column (Bio-Rad Laboratories, Hercules, CA, USA) packed with 15 ml Sephadex g100 (Sigma-Aldrich, St. Louis, MO, USA). Fractions of 1 ml with eluted from the column by washing with PBS (Gibco™, Invitrogen, Carlsbad, CA, USA). Eluates 3 to 9 were pooled as these contained EVs and samples were stored at -80°C until use.

## ***EVs from Ascaris suum***

Live adult *Ascaris suum* nematodes were obtained from pigs slaughtered at the Danish Crown abattoir in Herning, Denmark. Five worms, two males and three females, were put in a T175 flask and washed in 175 ml RPMI-1640 with 1X Antibiotic-Antimycotic (Thermo Fisher Scientific; Cat.: 15240062) and 1 µg/ml ciprofloxacin (Sigma; Cat.: 17850) (RPMI-Anti/Anti) in a total of four cycles of 15 minutes followed by three cycles of one hour of incubation at 37 °C. After washing, the worms were incubated in 175 ml RPMI-Anti/Anti for 72h in a 5% CO<sub>2</sub> incubator at 37 °C. The media containing excretory/secretory (ES) products from the worms was exchanged and collected every 24 hours. The collected ES products were stored at -80 °C. ES products from all three days were thawed at 4 °C and pooled to be concentrated 720 times with Amicon® Ultra-15 Centrifugal Filter Unit 10 kDa cut-off (Merck; Cat.: UFC901024). The concentrate was used for EV separation.

To separate EVs, two different methods were used: ultracentrifugation (UC) and size exclusion chromatography (SEC). Ultracentrifugation procedure: 500 µl of the concentrated ES products were transferred to polycarbonate ultracentrifuge tubes with cap assembly (Beckman Coulter; Cat.: 355603) and diluted with PBS 1X to a final volume of 10 ml. Total volume was centrifuged at 10000 xg for 30 minutes at 4°C at 10000 xg for 30 minutes at 4 °C (Beckman Coulter Optima L-80 XP Ultracentrifuge, TI 50 rotor kept at 4°). Supernatant (approx. 10 ml) was transferred to a new polycarbonate ultracentrifuge tube and centrifuged at 100000 xg for 70 minutes at 4°C (Beckman Coulter Optima L-80 XP Ultracentrifuge, TI 50 rotor kept at 4°C). The pellet was then dissolved in 10 ml of PBS 1X and re-centrifuged at 100000 xg for 70 minutes at 4°C. Final pellet was resuspended in 2 ml PBS 1X, transferred to an Eppendorf tube and stored at -80°C. SEC procedure: EVs were separated using qEVoriginal/70 nm columns from iZON (iZON Science Ltd; Cat.: SP1) according to manufacturing instructions using PBS 1X as buffer. Twenty-four fractions of 500 µl were collected. The fractions 7-10 were pooled as EV-containing fraction and stored at -80°C.

## ***EV characterization***

EV preparations from bovine milk and *Ascaris suum* were characterized for purity from protein contaminants and titrated by Colorimetric Nanoplasmonic Assay (CONAN) assay (Supplementary Table ST1). EV size distribution was in addition determined by Nanoparticle Tracking Analysis (NTA) for samples from *Ascaris suum* E/S (Supplementary Figures S6-S8). Protein composition was analyzed by Western blot. It is to note that the biochemical characterization can be performed only on bovine milk derived EVs, since no specific protein markers have been identified for *Ascaris suum* samples so far. The presence of EV-associated markers, and non-EV markers is presented in Supplementary Figure S9. Characterization protocol details and results are reported below.

## ***Surface Preparation and Sample Deposition***

All AFM experiments were performed on poly-L-lysine (PLL) coated glass coverslips. All reagents were acquired from Sigma-Aldrich Inc (www.sigmaaldrich.com) unless otherwise stated. Microscopy glass slides (15mm diameter round coverslips, Menzel Gläser) were cleaned in a sonicator bath (Elmasonic Elma S30H) for 30 minutes in acetone, followed by 30 minutes in isopropanol and 30 minutes in ultrapure water (Millipore Simplicity UV). Clean slides were incubated overnight in a 0.0001% (w/v) PLL solution at room

temperature, thoroughly rinsed with ultrapure water and dried with nitrogen. The water contact angle (1 $\mu$ l droplets at  $\sim 25^\circ\text{C}$ , measured with a GBX DigiDrop goniometer) of slides was  $26^\circ \pm 1^\circ$  prior to functionalization and  $20^\circ \pm 2^\circ$  after PLL deposition.

A 10  $\mu$ l-droplet of the vesicle-containing solution under study was deposited on a PLL-functionalized glass slide and left to adsorb for 10 minutes at  $4^\circ\text{C}$ , then inserted in the AFM fluid cell (see below) without further rinsing. The concentration of each vesicle-containing solution was adjusted by trial and error in successive depositions in order to maximize the surface density of isolated, individual vesicles and minimize clusters of adjoining vesicles.

### ***AFM setup***

All AFM experiments were performed in ultrapure water at room temperature on a Bruker Multimode8 (equipped with Nanoscope V electronics, a sealed fluid cell and a type JV piezoelectric scanner) using Bruker SNL-A probes (triangular cantilever, nominal tip curvature radius 2-12 nm, nominal elastic constant 0.35 N/m) calibrated with the thermal noise method [Hutter 1993].

### ***AFM Imaging***

Imaging was performed in PeakForce mode. In order to minimize vesicle deformation or rupture upon interaction with the probe, the applied force setpoint was kept in the 150-250 pN range. Lateral probe velocity was not allowed to exceed  $5\mu\text{m/s}$ . Feedback gain was set at higher values than those usually employed for optimal image quality in order to ensure minimal probe-induced vesicle deformation upon lateral contact along the fast scan axis.

This type of parameter optimization resulted in images with comparatively high noise levels in the empty areas of the surface ( $\leq 20\text{nm}$  peak to peak), but in which the height profiles of individual vesicles measured along both the slow and the fast scan axis could be fitted extremely well with circular arcs (Figure S1c). The average height value of all bare substrate zones was taken as the baseline zero height reference.

Image background subtraction was performed using Gwyddion 2.53 [Necas 2012]. Image analysis was performed with a combination of Gwyddion and custom Python scripts, but it can be easily carried out manually by only using functions included in Gwyddion and a spreadsheet.

### ***AFM force spectroscopy***

The mechanical characterization of vesicles via AFM force spectroscopy was performed following the approach recently described in [Vorselen 2017]. The sample was first scanned (see previous paragraph) to locate individual vesicles (Figure S1a). The chosen vesicle was then imaged (Figure S1b) at higher resolution ( $\sim 500 \times 500$  nm scan,  $512 \times 512$  points); its height profile along the slow scan axis was fitted with a circular arc only taking into account values 10nm above the bare substrate (typical fit  $R^2 \geq 0.95$ ). This procedure yielded, for each vesicle, an apparent fitted curvature radius  $R_c$  and a vesicle height value  $H_s$  (Figure S1c), which were corrected as described elsewhere [Vorselen 2017].

In principle, it would be sufficient to record the force/distance plot of just one approach/retraction cycle for each vesicle measured at its highest point, while avoiding membrane puncturing. In our hands however, this was practically impossible due to intrinsic piezo inaccuracy and drift, which imply a certain degree of

uncertainty on both the XY position at which the force curve is performed relative to the original image, and on the maximum applied force.

To overcome this limitation, we recorded a series of force/distance curves at multiple XY positions (typically around 64-100 curves arranged in a square array covering the vesicle initial location Figure S1b, green crosses) for each individual vesicle. In most cases, only a few curves showed the full mechanical fingerprint of an intact vesicle on both the approach and retraction cycles (Figure S1d), showing a linear deformation upon applied pressure and a tether elongation plateau during probe retraction. Of these, we first discarded those with probe-vesicle contact points ( $P_c$ ) occurring at probe-surface distances below vesicle height as measured by imaging ( $P_c < H_s$ , see previous paragraph). We then discarded traces in which the tether elongation plateau occurring during probe retraction did not extend beyond initial contact point. However, we relaxed this requirement for those natural vesicle samples on which obtaining clean tether plateaus was nearly impossible (see results and discussion section).

Remaining traces (typically 1-3 per vesicle) were analyzed to calculate vesicle stiffness ( $k_s$ ) and tether elongation force ( $F_T$ ). Multiple valid curves referring to the same vesicle resulted in very narrow distributions of both  $k_s$  and  $F_T$  (with average measured values taken as representative for each vesicle), while different vesicles of the same type showed much larger variations (see below). Membrane bending modulus ( $\kappa$ ) and internal pressurization ( $\Pi$ ) values were then calculated for each individual vesicle using its  $R_c$ ,  $k_s$  and  $F_T$  values as described in [Vorselen 2017].

### *Trigonometry calculations*

The contact angle value  $\alpha$  is always calculated from  $H_S$  and  $R_{Cap}$  as follows:

$$(1) \quad \alpha = 90 - \sin^{-1}((R_{Cap} - H_S)/R_{Cap})$$

$H_S$  is directly obtained from AFM images;  $R_{Cap}$  and  $A_S$  are calculated from  $H_S$  and  $R_{Proj}$  as follows:

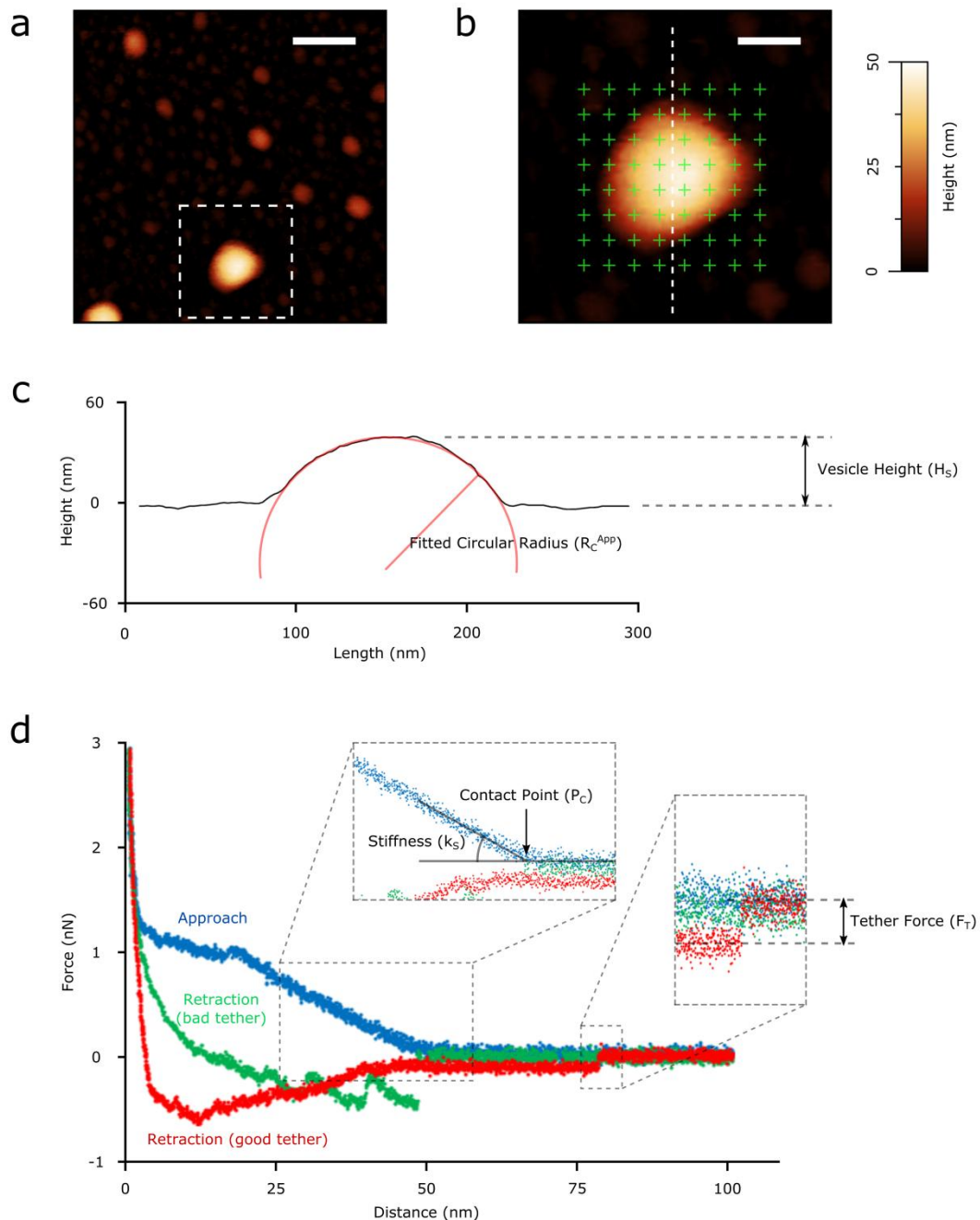
$$(2) \quad \text{If } R_{Proj} > H_S, R_{Proj} \approx A_{Cap} ; R_{Cap} = \frac{H_S^2 + R_{Proj}^2}{2H_S} ; A_S = \pi(2R_{Proj}^2 + H_S^2)$$

$$(3) \quad \text{If } R_{Proj} < H_S, R_{Proj} \approx R_{Cap} ; A_S = \pi H_S(4R_{Proj} - H_S)$$

Finally, the vesicle's diameter in solution  $D_L$ , assuming  $A_L = A_S$ , is

$$(4) \quad D_L = 2\sqrt{\frac{A_S}{4\pi}}$$

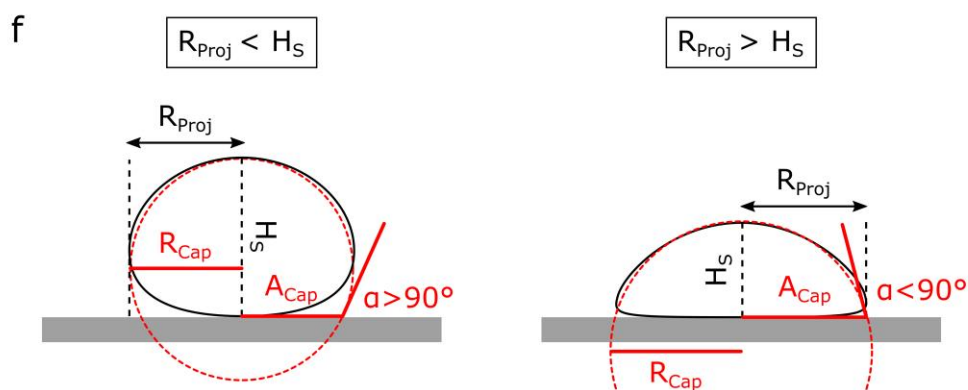
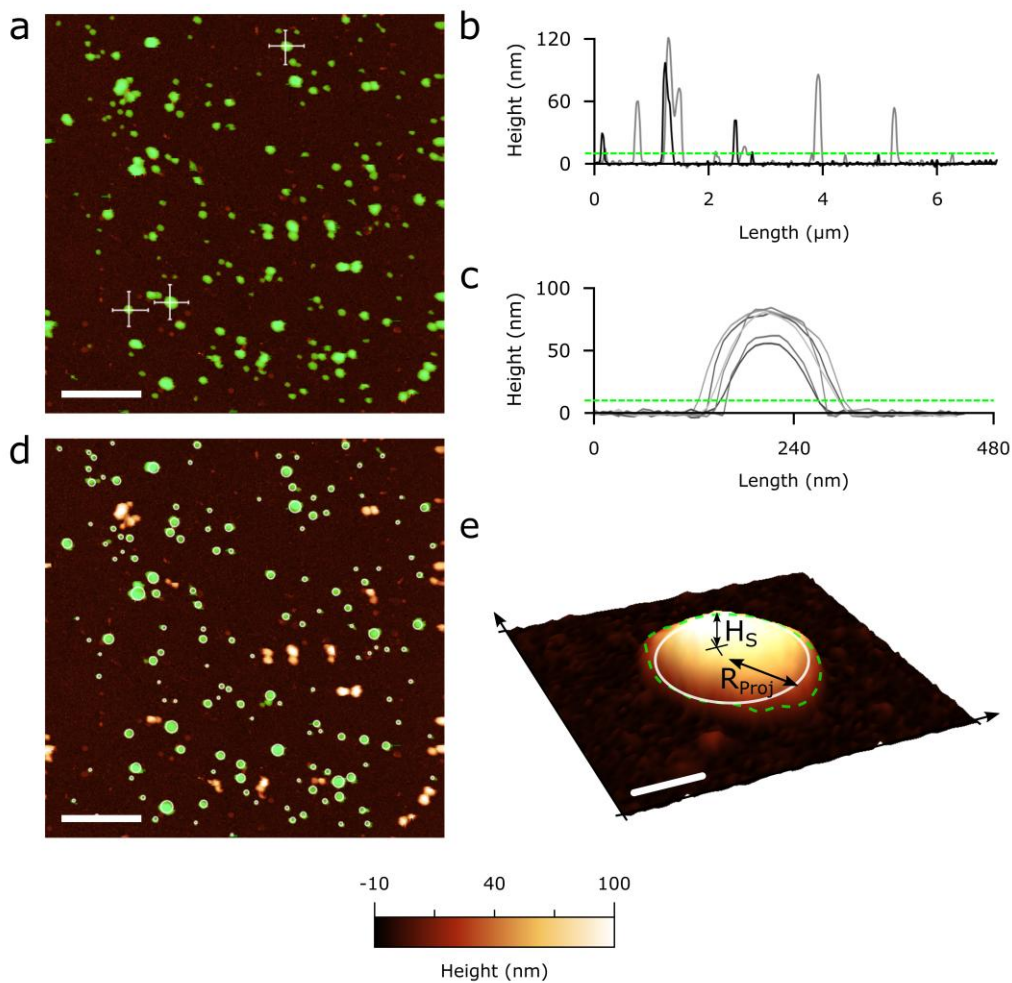
Supporting Figure S1



Mechanical characterization of individual vesicles by AFM force spectroscopy was performed following the approach recently suggested by Vorselen et al. [ref Vorselen 2017 in main text]. (a): As a first step, larger areas (scalebar 1  $\mu\text{m}$ ) were scanned to locate individual isolated vesicles (in this case, a POPC vesicle). (b): The selected vesicle was then imaged at higher resolution ( $\sim 500 \times 500$  nm scan, 512x512 points) to accurately characterize its morphology and to perform force spectroscopy approach/retraction cycles. To avoid intrinsic drifting problems of the piezo and also to gain a more robust estimate of the overall response of the vesicle, multiple indentations were performed following the points on a grid (green crosses) drawn on the vesicle and its surroundings. (c): The height profile along the slow scan axis is fitted with a circle to obtain the curvature radius  $R_c^{App}$  which is then corrected for tip convolution (see Figure S2)

and used in the normalization of the values of stiffness and internal pressure. Vesicle height  $H_s$  is also measured. (d): Typical force/distance curves recorded during approach and retraction FS cycles performed on a single vesicular object. In the approach (blue) curve, applied force remains zero until the tip first touches the vesicle at Contact Point  $P_c$ , then increases during vesicle indentation. All the curves that showed interactions at Distance values lower than the height  $H_s$  observed in the previous imaging step were discarded. According to CHM theory [main text refs Canham 1970; Helfrich 1973], the initial mechanical response of the vesicle to indentation is elastic and linear; the application of a linear fit to this portion of the curve yields the stiffness  $k_s$  of the vesicle. The red trace describes the retraction of the tip from the sample and is characterized by the formation of a membrane tether that is pulled by the tip beyond the initial contact point ending with a sharp return to the initial zero force value. The force value measured before this rapid variation is the tether elongation force  $F_T$ . All the retraction curves that did not resemble the event of tether formation described by the red trace were not considered in the analysis. Obtaining force curves unambiguously showing tether elongations is one of the main issues for the successful application of this FS method to EVs. As exemplified by the green trace, in most retraction traces following the indentation of an EV the presence of abundant membrane proteins and/or peptidoglycans causes the appearance of multiple unfolding/detachment/rupture events (absent in synthetic liposomes) which often avoid the formation and/or identification of single membrane tethers.

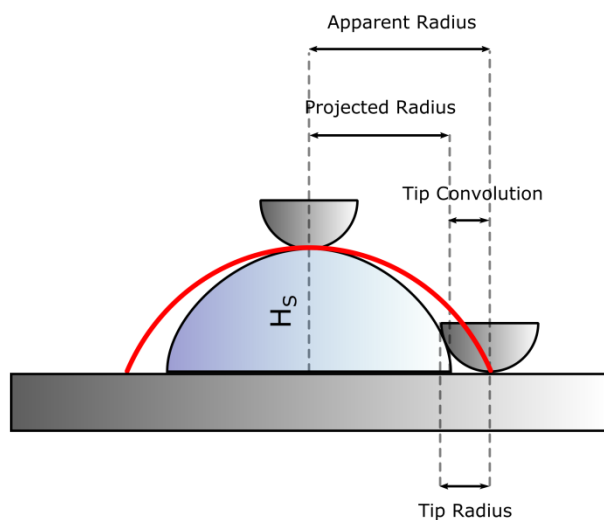
Supporting Figure S2



AFM imaging and morphometry analysis. (a): representative AFM micrograph of a DPPC liposome sample deposited on a PLL-functionalized substrate. Scalebar = 1 $\mu$ m. Correct background subtraction is crucial to successive image analysis steps (see materials and methods) and is first checked by plotting height profiles measured along the two diagonals of the whole image (b): after proper flattening, diagonal profiles must show a flat baseline centered at height=0 with positive features. To minimize probe-induced vesicle deformation, imaging should be preferentially performed at low applied load (<250 pN) and high feedback gain (see main text, materials and methods). (c): Profiles of putative vesicles measured along fast and slow

scan axes (panel a, white lines) should be roughly symmetrical and superimposable, indicating minimal mechanical perturbation due to scanning. Circular arcs are typically able to fit to random profiles of vesicles with an  $R^2 \geq 0.99$  when discarding the substrate-proximal region (see below). (a,b,c): based on the observed signal/noise ratio, an height threshold (green mask in panel a, dashed line in panels b and c) is utilized to separate features subjected to successive analysis steps from the background. A threshold of 10 nm was used in most cases. (d): If present, manifestly non-globular impurities or imaging artifacts are manually excluded from the analysis. Mutually- or edge-touching globular objects are also discarded. For each remaining globule (green mask), the largest inscribable disc is then plotted (white circles), discarding objects having inscribed disc radii below 10 nm. (e): Each remaining object is considered a putative vesicle, and its morphology is parametrized with two quantities measured from its AFM image: the corrected (see Figure S2) radius  $R_{proj}$  of the largest possible disc (white circle) inscribed within the boundary delimited by the height threshold (green dashed line), and the highest Z value occurring within it,  $H_s$ . Scalebar is 75 nm. (f): Geometrical approximation of the spheroid shape of a surface-adhered vesicle with a spherical cap having height  $H_s$ , surface radius  $A_{cap}$  and spherical radius  $R_{cap}$ . While  $H_s$  is always directly measured on the AFM image (see panel e),  $R_{cap}$  and  $A_{cap}$  are calculated from as follows: if  $R_{proj} < H_s$ ,  $R_{proj}$  is taken as a good approximation of  $R_{cap}$ ; and when  $R_{proj} > H_s$ ,  $R_{proj}$  is taken as a good approximation of  $A_{cap}$ . In all cases, contact angle  $\alpha$  is then calculated via simple trigonometry calculations (see above).

### Supporting Figure S3

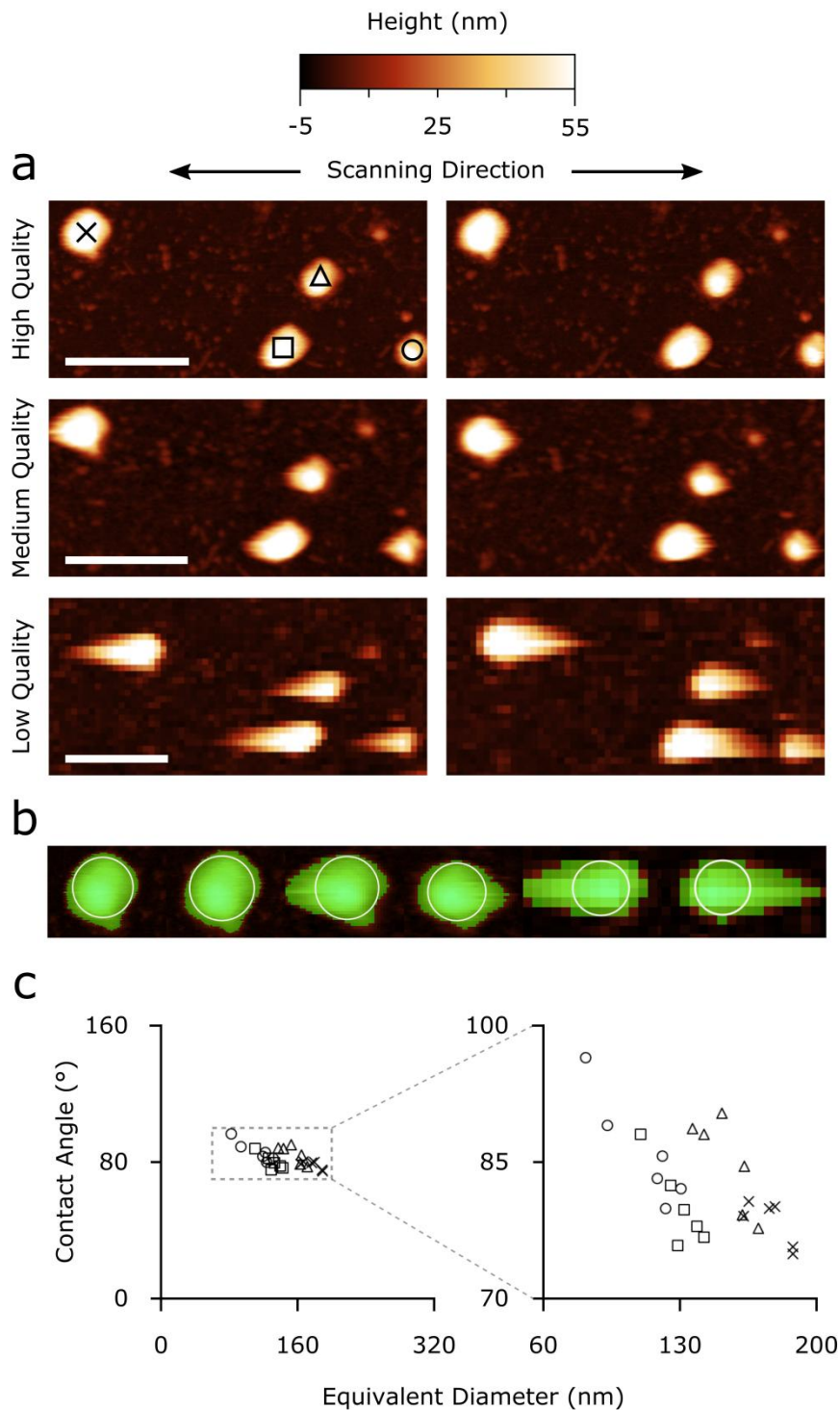


Influence of AFM probe on the nanomechanical characterization of vesicles. The position of a vesicle on a Contact Angle vs. Diameter plot is determined by the  $H_s$  and  $R_{\text{proj}}$  values measured on its AFM image. While the measurement of  $H_s$  is only affected by force setpoint and feedback gain (see main text),  $R_{\text{proj}}$  is affected by tip convolution. Due to this, maximum inscribed disc radii values measured on the AFM image should be regarded as ‘apparent radii’, resulting from the sum of  $R_{\text{proj}}$  plus a tip contribution. This tip ‘broadening’ contribution is variable in entity, and linked to the exact shapes of the tip (its curvature radius at the apex being the most important) and the vesicle (in particular,  $H_s$ ). A clear indication of excessively large tip convolution is a non-circular profile of several vesicular objects in an image; it is not advised to apply image analysis to images where this occurs. Circular profiles (see main text image 2c) can only result from the convolution of two objects having circular shapes along the scanning direction; recording two perpendicular circular profiles on the same object is thus indicative of the fact that the tip is effectively behaving as a hemisphere, and that the largest possible overestimation of  $R_{\text{proj}}$  coincides with its apex curvature radius. In any case, the largest broadening effect occurs at the base of the vesicle, which is not included in our image analysis procedure since it only takes into account those portions of objects being above a height threshold (see main text Figure 2a, b and c). This reduces the maximum impact of tip convolution on successive analysis steps to a fraction of the probe’s curvature radius. The nominal tip radii of most commercially available ‘sharp’ AFM tips (e.g. from 2 to 12 nm for the Bruker SNL probes employed in this study) limits the maximum possible overestimation of  $R_{\text{proj}}$  to ~10 nm in the worst case scenario for vesicles with  $\alpha \geq 90^\circ$ . Progressively shallower vesicles would be less affected; the total result being a ~5% underestimation of  $\alpha$  for a ‘typical’ vesicle with  $H_s = 50$  nm in the worst possible scenario.

These considerations suggest that, by using tips with apex curvature radii  $\leq 10$  nm and by taking the opportune precautions detailed in the materials and methods section of main text, one can in most cases neglect tip de-convolution. It is important to note that several pieces of information obtained from a Contact Angle vs. Diameter scatterplot (e.g. the presence of contaminants, the attribution of items in a horizontally elongated cluster to vesicle-like mechanical behavior, the relative position of clusters) are unaffected by tip convolution. We only advise tip convolution correction in those cases in which the quantitative readout of  $\alpha$  is crucial (e.g. for the quantitative estimation of  $k_s$ ), and if a reliably sharp tip is unavailable. In these cases, it would be possible to correct  $R_{\text{proj}}$  values by simply adding an internal standard

to the sample. This internal standard could be constituted by monodisperse rigid spherical nanoparticles, which could be singled out and used to estimate XY tip convolution, or a synthetic liposome with a previously characterized  $\alpha$  value. The latter would appear as an additional horizontal cluster in the  $\alpha$ /size scatterplot; apparent  $R_{proj}$  values would then be adjusted by different tip radius values until the reference cluster average  $\alpha$  coincided with the expected value.

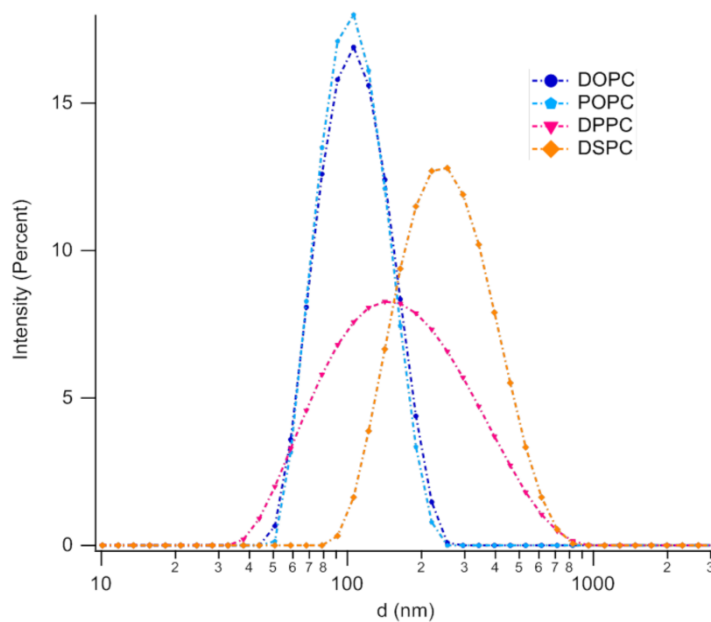
Supporting Figure S4



Robustness of the image analysis procedure with respect to imaging quality. Quantitative measurements of  $\alpha$  are based on two parameters obtained from AFM images: vesicle height  $H_s$  and Projected Radius  $R_{proj}$ . While it is of course advised to perform the analysis on AFM images of the best available quality (with respect to resolution, feedback setting, and applied force setpoint: see main text), we found that both  $H_s$  and  $R_{proj}$  are only marginally affected by image quality. (a): The two main parameters affecting AFM image quality are feedback gain and resolution (here strictly intended as number of recorded points). We show six

AFM scans on the same four individual *Ascaris* EVs performed in different instrumental conditions. Images in the left and right column respectively correspond to ‘trace’ (toward cantilever apex) and ‘retrace’ (toward cantilever base) fast scan axis directions. Images in the top, middle and bottom rows were acquired with progressively worse imaging quality. Top row: 512x512 points, best feedback setting (vesicles have symmetrical profiles). Mid row: 256x256 points, suboptimal feedback setting (vesicles start to show slow feedback artifacts, elongated ‘tails’ start to appear in the scanning direction). Bottom row: 128x128 points, worse feedback setting (vesicles have long feedback artifacts in the scanning directions). All scalebars are 400nm. (b): Detail of the six scans performed on the vesicle marked with an “X” in panel a. The zone above the selected height threshold is highlighted in green; it is easy to notice how its horizontal deformation caused by feedback artifacts has a limited impact on the maximum inscribed disc radius used to calculate  $R_{proj}$  (white circles). Similarly, reduced resolution has a very limited impact on the maximum height value corresponding to  $H_s$ . (c):  $\alpha$ /size plot of the four vesicles shown in panel a. Each vesicle is marked with the same symbol used in panel a, and plotted at the six slightly different coordinates resulting from image analysis of the six scans of panel a. Pooling the six measurements performed on each vesicle and calculating their variance allows the dispersion of both  $\alpha$  and  $D_L$  values induced by image quality to be estimated.  $R_{proj}$  and  $H_s$  values obtained from the worst images cause deviations of ~5% in  $\alpha$  and ~20% in  $D_L$  with respect to the best ones. Needless to say, it’s advisable to always use the best attainable image quality, in particular for quantitative correlation studies such as the one described in main text under the heading “Quantitative estimation of EV stiffness from AFM images”.

Supporting Figure S5



Lipid composition	Dh (nm)	PDI	Zeta Potential (mV)
DOPC	115 ± 5	0.09 ± 0.01	-11 ± 3
POPC	110 ± 8	0.10 ± 0.05	-9 ± 2
DPPC	170 ± 20	0.34 ± 0.05	-10 ± 3
DSPC	290 ± 20	0.20 ± 0.03	-11 ± 4

Dynamic Light Scattering (DLS) and Zeta Potential characterization of liposomes: (a) Graph reporting the size distribution, as contribution to the scattered intensity, of each lipid composition, as obtained from DLS measurements; (b) Table summarizing average hydrodynamic diameter (Dh) and polydispersity index (PDI) of the lipid vesicles, obtained from DLS analysis, and Zeta Potential values measured for each liposomal dispersion. DLS and Zeta Potential measurements have been performed on a Laser Doppler Microelectrophoresis (Malvern Zeta Sizer Nano Z), enabling the calculation of electrophoretic mobility and, from this, zeta potential and zeta potential distribution, through the laser interferometric technique M3-PALS (Phase analysis Light Scattering). The measurements have been performed at 25°C. The reported values are an average of three measurements performed on each sample. Measurements were performed at the PSCM Lab (EPN Campus, Grenoble, France). From the reported data it is clearly highlighted that lipid vesicles from DPPC and DSPC (i.e., with a higher stiffness at r.t.) tend to be characterized by larger average sizes and higher polydispersity. All vesicles dispersions in water are characterized by similar, and slightly negative, zeta potential values.

## *Additional EV characterization*

### *EV preparations purity assessment*

EV preparations from bovine milk and *Ascaris suum* excretory/secretory products were checked for purity from protein contaminants by the COlorimetric NANoplasmonic (CONAN) assay, which exploits the nanoplasmonic properties of colloidal gold nanoparticles (AuNPs) and their peculiar interaction with proteins and lipid bilayers [Maiolo 2015]. The CONAN assay used in this work consisted of a 6 nM Milli-Q water solution of 14 nm diameter AuNPs. AuNPs were synthesized by the Turkevich's method. The experiments were conducted and data analyzed using the protocols described in [Zendrini 2019]. All the UV/vis/NIR absorption spectra were collected with an Ensign multimode plate reader (PerkinElmer), which allowed collection of the spectra on samples of 100  $\mu$ L final volume.

The assay consists of an aqueous solution of bare AuNPs at 6 nM concentration. When mixed with pure EV formulations, the AuNPs cluster on the EV membrane, whereas in EV formulations which contain exogenous protein contaminants (EPCs) the AuNPs are preferentially cloaked by such EPCs (an AuNP-EPC corona forms), which prevents AuNPs from clustering to the EV membrane. When AuNPs cluster (are in tight proximity), their localized surface plasmon resonance (LSPR) red shifts and broadens, resulting in a color change of the AuNP solution from red to blue, which can be accurately monitored through UV-vis spectroscopy. The assay red shift is therefore directly related to the purity grade of the added EV formulation and can be conveniently quantified by describing the AuNP UV/vis/NIR absorption spectra with the nanoparticle Aggregation Index (AI), defined as the ratio between the absorbance intensity at the LSPR peak and the intensity at 650+850 nm [Busatto 2018; Mallardi 2018]. For all the analyzed EV formulations separated as described in the main text, the AI values resulted in around 20% of the reference AI of the initial assay (i.e., the dispersed AuNP solution). This proves the EV formulations contained negligible amounts of EPCs. Results reported indicate that the AI for the assayed EV formulation is around 20% of the AI of the starting assay. According to the limit of detection for protein contaminants reported in [Zendrini 2019], this indicates the samples contain an overall amount of exogenous contaminants  $\leq 50$  ng/ $\mu$ L.

### *EV titration*

In the case negligible amount of proteins in EV preparations ( $< 50$  ng/ $\mu$ L) the aggregation index (AI) of the CONAN assay is proportional to the EV number density. We exploited the assay to determine EV total molar concentration (Table ST1) measuring the AI of a POPC liposome calibration curve at known molar concentrations (from 0.8 to 12.5 nM) and interpolating EV AI to the curve. Full details are given in [Busatto 2018 and Zendrini 2019].

### Supplementary Table S1

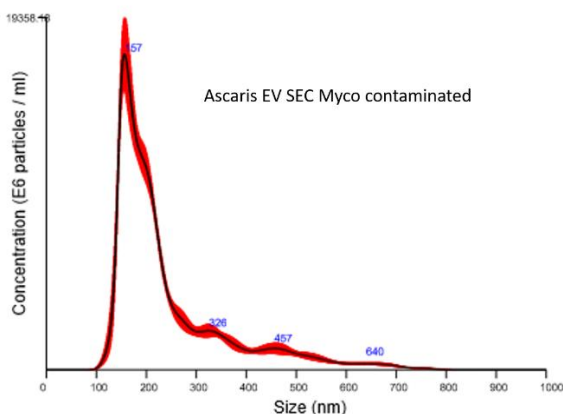
EV sample	EV total molar concentration (mol/L)
SEC+Myco	7.07 E-08
UC+Myco	5.64 E-08
SEC myco free	1.00 E-08
Bovine Milk	4.25 E-07

**Table S1:** EV total molar concentration. UC+Myco: *Ascaris suum* EV separated from mycoplasma contaminated medium. Separation protocol: Ultracentrifugation (UC). SEC+Myco: *Ascaris suum* EV separated from mycoplasma contaminated medium. Separation protocol: size exclusion chromatography (SEC). SEC+Myco: *Ascaris suum* EV separated from mycoplasma free medium. Separation protocol: size exclusion chromatography (SEC). Bovine milk: EV separated from bovine milk.

### Nanoparticle Tracking Analysis

EVs size distribution of *Ascaris suum* samples was additionally determined with Nanoparticle Tracking Analysis (NTA). EV separated after ultracentrifugation protocol (UC) or size exclusion chromatography (SEC, fractions 7-10) (see main text for details) were analyzed with a Nanosight NS300 system (Malvern) coupled with a Nanosight syringe pump (Malvern) [using 405 nm wavelength (blue)]. Before any sample analysis, the system was quality checked by measuring a suspension of 100 nm polystyrene beads. In brief, PBS-diluted samples (final volume 1 ml) were injected into the sample chamber using a syringe and the microscope objective was adjusted in order to obtain a clear picture of particles within the beam. Analysis parameter: Flow rate: 10; Temperature: 23°C; Screen gain: 1; Viscosity: Water; Camera level: 10. For each sample, five measurements were performed with a duration of 60 seconds for each repeat/frame. The data were analyzed using NTA software version 3.2.

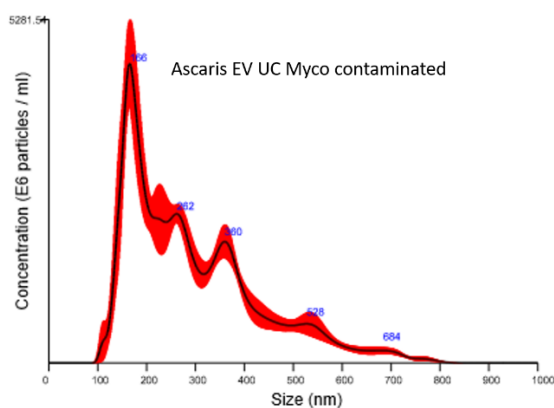
### Supporting Figure S6



Average finite track length adjustment (FTLA) Concentration/Size graphs for NTA analysis of particles of *Ascaris* EVs separated with SEC. Medium contaminated with mycoplasma. Red error bars indicate +/- 1 standard error of the mean. Mode 157.5 +/- 3.5 nm. It is important to note that the size of mycoplasma

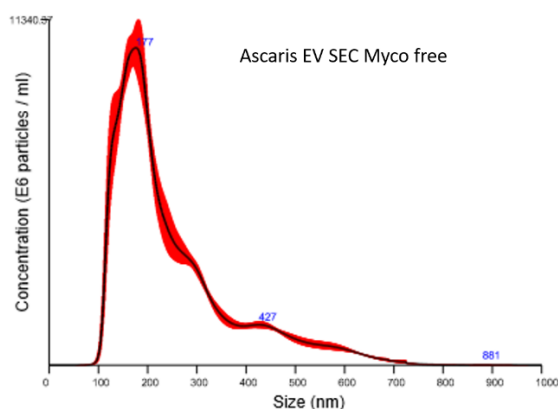
contaminants is, on average, smaller than 50 nm (as can be seen by looking at the vertical cluster in Fig. 3d of the main text); making it challenging to be revealed by NTA techniques, which usually present a limit of detection around 30 – 50 nm for EVs and protein aggregates [Bohren 2007].

### Supporting Figure S7



Average finite track length adjustment (FTLA) Concentration/Size graphs for NTA analysis of particles of Ascaris EVs separated with UC. Medium contaminated with mycoplasma (see fig S6 caption for additional discussion). Red error bars indicate +/- 1 standard error of the mean. Mode 164.7 +/- 8.4 nm.

### Supporting Figure S8



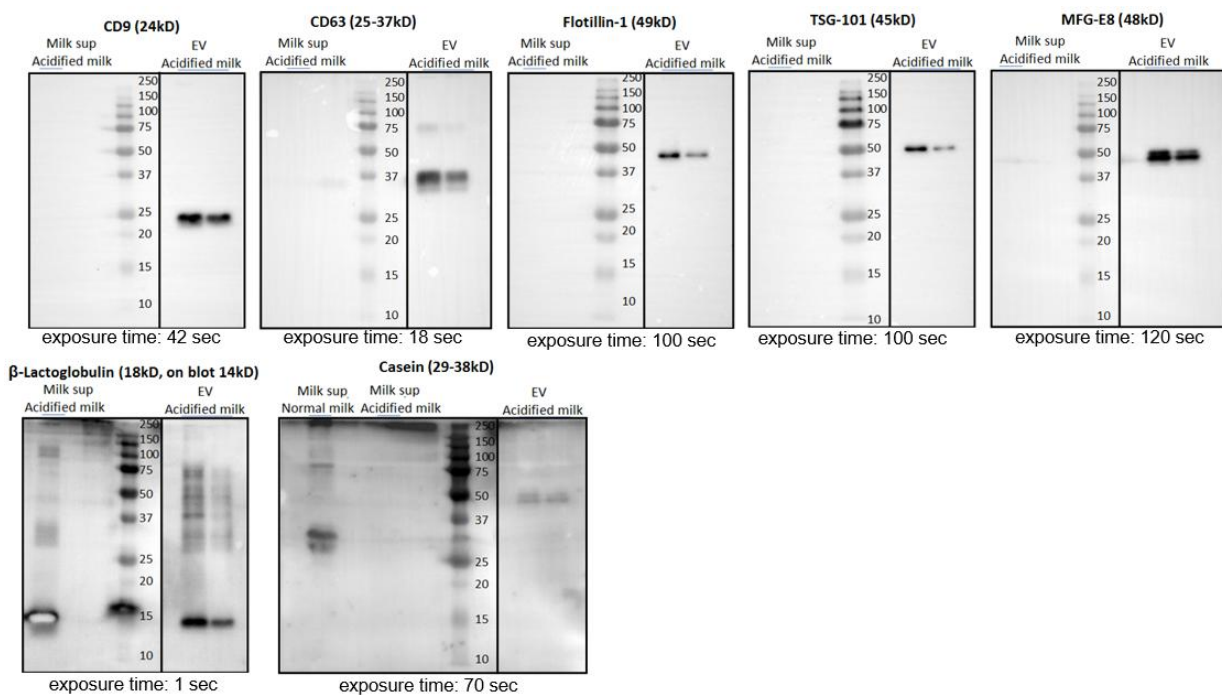
Average finite track length adjustment (FTLA) Concentration/Size graphs for NTA analysis of particles of Ascaris EVs separated with UC. Medium not contaminated with mycoplasma. Red error bars indicate +/- 1 standard error of the mean. Mode 166.4 +/- 6.3 nm

### EV biochemical characterization

For biochemical analysis purified EV samples from bovine milk were pelleted at 100000 xg for 65 minutes (in a Beckman Coulter Optima Max-XP with a TLA-55 rotor) in polyallomer microcentrifuge tubes (Beckman) and the pellet was resuspended in sample buffer (62.5 mM Tris pH 6.8, 2% SDS, 10% Glycerol). Samples were run on a 12.5% SDS-PAGE gel in order to separate proteins. The separated proteins were transferred onto PVDF membranes and blocked in PBS containing 0.2% fish skin gelatin (Sigma-Aldrich) and 0.1%

Tween-20. Proteins were detected by immunoblotting using rabbit-anti-human-MFG-E8 (Sigma HPA002807, dilution 1:1000); mouse-anti-bovine-CD63 (BioRad MCA2042G, dilution 1:2000); mouse-anti-human CD9 (Biolegend 312102, clone HI9a, dilution 1:1000); mouse-anti-human-Flotillin (BD 610821, clone 18, dilution 1:500 and the sample was reduced with DTT +  $\beta$ -mercapthoethanol); mouse-anti-human-TSG-101 (SC-7964, dilution 1:100 and the sample was reduced with DTT +  $\beta$ -mercapthoethanol); rabbit-anti-bovine Lactoglobulin- $\beta$ -HRP (Ab112894, dilution 1:1000); rabbit-anti-bovine Casein (GTX37769, dilution 1:500). Goat anti-mouse-HRP (Jackson Immuno Research, Suffolk, UK; 1:10000) was used as secondary antibody. HRP conjugated antibodies were detected using SuperSignal West Dura Chemiluminescent Substrate (Thermo Scientific, Landsmeer, Netherlands) and ChemiDoc XRS and Image Lab 5.1 (Bio-Rad) (Figure S8).

### Supporting Figure S9



Western blot characterization of purified milk EVs for CD9, CD63, Flotillin-1, TSG-101 and MFG-E8. Non EV-enriched proteins  $\beta$ -Lactoglobulin and  $\beta$  casein were included for characterization. For casein, a non-acidified (normal milk) sample was included to show the presence of casein in milk, as compared to acidified milk. Note that  $\beta$ -Lactoglobulin is predicted to be 18 kDa (which was observed in milk supernatant) but the band is lower in EVs. EV samples were technical duplicates as these were isolated from the same raw milk sample.

## Supplementary References

- [Bohren 2007]: Bohren CF, Huffman DR. "Absorption and scattering by a sphere", in: Bohren CF, Huffman DR, editors. Absorption and scattering of light by small particles. Weinheim: Wiley-VCH Verlag GmbH; 2007. pp. 83–129.
- [Busatto 2018]: Busatto S, Giacomini A et al. "Uptake Profiles of Human Serum Exosomes by Murine and Human Tumor Cells through Combined Use of Colloidal Nanoplasmonics and Flow Cytofluorimetric Analysis" *Anal. Chem* 90, 7855-7861 (2018)
- [Faria 2018]: M. Faria, M. Bjornmalm et al. "Minimum information reporting in bio-nano experimental literature" *Nat Nanotechnol* 13 (2018)
- [Hutter 1993]: J. L. Hutter, J. Bechhoefer, "Calibration of Atomic-Force Microscope Tips" *Rev Sci Instrum* 1993, 64. 1868-1873
- [Maiolo 2015]: Maiolo D, Paolini L et al. "Colorimetric nanoplasmonic assay to determine purity and titrate extracellular vesicles" *Anal. Chem* 87, 4168-76 (2015)
- [Mallardi 2018]: Mallardi A, Nuzziello N et al. "Counting of peripheral extracellular vesicles in Multiple Sclerosis patients by an improved nanoplasmonic assay and dynamic light scattering" *Colloids Surf B Biointerfaces* 168, 134-142 (2018)
- [Necas 2012]: D. Necas, P. Klapetek, "Gwyddion: an open-source software for SPM data analysis" *Cent Eur J Phys* 2012, 10. 181-188
- [Skliar 2018]: Skliar M, Chernyshev VS et al. "Membrane proteins significantly restrict exosome mobility" *Biochem. Biophys. Res. Comm.* 501, 1055e1059 (2018)
- [Thery 2018]: C. Thery, K. W. Witwer et al. "Minimal information for studies of extracellular vesicles 2018 (MISEV2018): a position statement of the International Society for Extracellular Vesicles and update of the MISEV2014 guidelines" *J Extracell Vesicles* 7 (2018)
- [Van Deun 2017]: J. Van Deun, P. Mestdagh et al. "EV-TRACK: transparent reporting and centralizing knowledge in extracellular vesicle research" *Nat Methods* 14 (2017)
- [Vorselen 2017]: D. Vorselen, F. C. MacKintosh et al. "Competition between Bending and Internal Pressure Governs the Mechanics of Fluid Nanovesicles" *Acs Nano* 2017, 11. 2628-2636
- [Zendrini 2019]: Zendrini A, Paolini L et al. "Augmented COLORimetric NANoplasmonic (CONAN) Method for Grading Purity and Determine Concentration of EV Microliter Volume Solutions" *Front. Bioeng. Biotechnol.*, 7, 452 (2020)